Hybrid Tuned Center Difference - WENO Method for Large Eddy Simulations in the Presence of Strong Shocks

D.J. Hill and D.I. Pullin

Graduate Aeronautical Laboratories, California Institute of Technology, Pasadena, California 91125

Abstract

We develop a tuned center-difference (TCD) scheme optimized for large-eddy simulations (LES) simulations using a method proposed by Ghosal. For LES of weakly compressible decaying turbulence, these optimized stencils are shown to provide superior performance when compared to higher-order centered schemes with the same stencil width. A hybrid method combining the TCD stencil with a weighted essentially non-oscillatory (WENO) method is then constructed for use in the LES of strongly compressible, shock-driven flows. The user-specified, optimum WENO weights are chosen to match those of the TCD scheme. It is expected that these weights will be achieved automatically in regions of smooth flow away from shocks, but in practice a switch is found to be necessary. The hybrid TCD-WENO scheme is shown to work well for unsteady gas-dynamic flows in one and two dimensions.

Key words: compressible turbulence, LES, hybrid methods, center difference

1 Introduction

It has been observed [5,12] that the success of Large Eddy Simulations (LES) depends not only on the subgrid stress model employed, but also on the numerical approximation of derivatives in the advection terms on the resolved scales. The most successful approaches have utilized spectral methods or the spectral-like methods comprised of the class of high-order compact (Padé) finite difference approximations. Both of these highly accurate methods are global in nature and are characterized by their fidelity in phase across a wide range of scales. Spectral methods, of course, have zero phase errors, while compact schemes have substantial phase errors only for the smallest resolved scales [9]. Unfortunately the nonlocal dependence of these approaches renders them

ill-suited for a variety of problems such as flows containing strong shocks and flows in complex geometries. Furthermore, they can introduce complications and non-optimal efficiency when implemented in parallel codes, or when integrated with techniques such as adaptive mesh refinement (AMR). Attempts (eg [3] & [6]) have been made to use spectral methods in the calculation of compressible Euler flows in the presences of strong shocks, in which cases additional viscosity is needed to insure stability and post processing techniques are used to address ringing. While this approach is interesting, it has yet to be shown to be well suited for LES.

In the first part of this paper we investigate the role of the phase errors relative to formal order of accuracy in the resolved-scale calculations of LES. This is done by the development of explicit, second-order 5-point and fourth-order 7-point centered finite-difference stencils optimized for LES. Examples of weakly compressible turbulence calculations are presented and favorable results are found when compared against direct numerical simulations (DNS). These stencils, being local in nature and computationally inexpensive, have certain advantages over their nonlocal counterparts. In the second part we exploit some of these properties in formulating a hybrid center-difference-WENO scheme for the study of compressible turbulence in the presence of shocks.

2 Tuned Center-Difference (TCD) Stencil for LES

We first discuss, in the context of explicit centered stencils, the relation between formal order of accuracy and bandwidth fidelity. This is followed by a description Ghosal's [4] measure of truncation error resulting from the discretized Navier-Stokes equations applied to turbulent flows, which is then used in optimizing bandwidth at the expense of order of accuracy. We refer to such stencils as tuned center-difference (TCD). Finally we present examples of LES calculations using these new stencils, and good agreement with DNS is obtained.

2.1 Wide Center-Difference (Free Parameter)

In using a finite-difference representation of the first derivative, there are two related but different concepts in analyzing the fidelity of a numerical difference operator: formal order of accuracy and the dispersion relation. Taylor series analysis is a local tool that provides the order of accuracy, while Fourier analysis is used to investigate the dispersion relation. Utilizing a concept often called bandwith optimization in aero-acoustics [22] we show that formal accuracy can be sacrificed in exchange for better dispersion properties in the construction

of an explicit center-difference scheme to represent the first derivative. Recognizing that practical and computational concerns are best served by relatively compact stencils, attention is presently restricted to stencils of at most seven points. Let $\triangle x$ to be the uniform grid spacing and define the general center-difference operator $\mathbf{D}$ as

$$\mathbf{D}f(x) = \frac{1}{\triangle x}\sum_{j=1}^{j=3} d_j(f(x+j\triangle x) - f(x-j\triangle x)). \tag{1}$$

Then by standard Taylor series expansion about $\triangle x = 0$,

$$\begin{aligned}\mathbf{D}f(x) = (2d_1 + 4d_2 + 6d_3)\left(\frac{df}{dx}\right)_0 + (\frac{1}{3}d_1 + \frac{8}{3}d_2 + 9d_3)\triangle x^2\left(\frac{d^3f}{dx^3}\right)_0 \\ + \big(\frac{1}{60}d_1 + \frac{8}{15}d_2 + \frac{81}{20}d_3\big)\triangle x^4\left(\frac{d^5f}{dx^5}\right)_0 + O(\triangle x^6),\end{aligned} \tag{2}$$

where the derivatives of $f(x)$ are evaluated at $\Delta x = 0$. By construction, any scheme with constant coefficients which satisfies $2d_1 + 4d_2 + 6d_3 = 1$ is an approximation to the first derivative. For a given set of coefficients d_j, the next nonzero term in the expansion defines the formal order of accuracy of the operator. For example, the choice of $d_1 = 3/4$, $d_2 = -1/10$ and $d_3 = 1/60$ leads to the standard sixth-order 7-point stencil, and $d_1 = 2/3$, $d_2 = -1/12$ with $d_3 = 0$ produces the common fourth-order, 5-point stencil.

An alternate approach to measuring the fidelity of an approximate derivative is to examine the eigenvalues of resulting operator. In the motivational context of a first order wave equation, this is equivalent to studying the dispersion relation of the approximate (spatially discrete) equation. Assuming for simplicity, periodicity over the spacial domain, single Fourier mode analysis of the linear operator results in

$$\mathbf{D}\exp(\mathbf{i}\kappa x) = \mathbf{i}\tilde{\kappa}(\kappa)\exp(\mathbf{i}\kappa x), \tag{3}$$

where κ is wavenumber and $\tilde{\kappa}(\kappa)$, which defines the dispersion relation for the operator, is referred to as the modified wavenumber. A method has spectral accuracy over the resolved scales if $\tilde{\kappa}(\kappa) = \kappa$, while the spectral-like methods [9] approximate κ well for all but the highest resolved wavenumbers. Similarly one finds for $\mathbf{D}$ defined in (1) that

$$\tilde{\kappa}(\kappa) = \frac{1}{\triangle x}[2d_1\sin(\kappa\triangle x) + 2d_2\sin(2\kappa\triangle x) + 2d_3\sin(3\kappa\triangle x)], \tag{4}$$

which, like Padé derivatives, tends to zero for the highest resolved wavenumbers.

As a consequence of the centered nature of (2), $\tilde{\kappa}(\kappa)$ is purely real, implying there are no dissipative errors when applied to the first-order wave equation

or, as is the case in LES calculations, the advection terms in the momentum equation. Note that there are dispersion errors, particularly for the smaller resolved scales. One could increase the number of points in the stencil so that $\tilde{\kappa}$ includes more terms in this sin-series for κ, but in doing so the advantages of a small, spatially compact explicit stencil, would be lost.

The approach taken in this paper is to relax the order of accuracy requirements by insisting only that the 7-point stencil be fourth-order accurate and that the 5-point stencil be second-order. This relaxation, while retaining the centered form of the stencils, provides a scalar degree of freedom to be exploited in improving the modified wavenumber behavior. For the 7-point stencil, if $\alpha = d_3$ is taken to be a free parameter, then the requirement of fourth-order accuracy leads to

$$\begin{aligned} d_1 &= \frac{2}{3} + 5\alpha, \\ d_2 &= -\frac{1}{12} - 4\alpha, \end{aligned} \tag{5}$$

while for the 5point stencil $d_3 = 0$, take $\alpha = d_2$ and the constraint of second-order accuracy gives

$$d_1 = \frac{1}{2} - 2\alpha. \tag{6}$$

For such stencils, different choices of α can have substantial affects on the modified wavenumber $\tilde{\kappa}(\kappa)$. In the following section a measure is discussed that allows for a rational choice of α for LES calculations.

2.2 Ghosal Truncation Error

For general applications, several optimization procedures have been suggested for improving the bandwidth of $\tilde{\kappa}$ based on minimizing weighted integral measures of the the error $(\kappa - \tilde{\kappa})\omega(\kappa)$, [18,22,23]. A certain degree of freedom in the choice of the weighting function $\omega(\kappa)$ is introduced by such methods. The approach followed in this paper obviates the need to experiment with the weighting function by utilizing an analysis of the governing equations in the presence of turbulent flow as a method of bandwidth tuning.

To better understand the role of dispersion error and modified wave number behavior in LES calculations, Ghosal [4,5] formulated an expression for the error in the resolved scale kinetic energy produced by one time step of the Navier-Stokes equation discretized by methods producing known modified wavenumbers, for example, explicit differences, Padé schemes, and spectral methods. To derive this expression for the truncation error $\mathcal{E}^{(\mathrm{FD})}(\kappa, \tilde{\kappa}(\kappa))$, Ghosal assumed that the flow field itself represents homogeneous incompressible isotropic turbulence with a velocity (energy) spectrum $E(\kappa)$ well described

by the Von-Kärman form

$$E(\kappa) = \frac{a\kappa^4}{(b+\kappa^2)^{17/6}}, \tag{7}$$

which has the desired properties $E(\kappa) \sim \kappa^4$ as $\kappa \to 0$ and $E(\kappa) \sim \kappa^{-5/3}$ as $\kappa \to \infty$.

While the reader is referred to Ghosal [4] for details, for completeness we presently summarize the basic argument and quote the important result. Beginning with the incompressible Navier-Stokes equations, formally written as $\partial_t \vec{u} = \mathcal{N}\vec{u}$, an equation for the evolution of the error $\vec{e} \equiv \mathcal{P}\vec{u} - \vec{u_0}$ on the resolved scales is formed

$$\frac{\partial \vec{e}}{\partial t} = \mathcal{N}_0 \mathcal{P}\vec{u} - \mathcal{N}_0 \vec{u}_0 + (\mathcal{P}\mathcal{N} - \mathcal{N}_0\mathcal{P})\vec{u}, \tag{8}$$

where $\vec{u}$ and $\mathcal{N}$ represent the exact velocity field and the (nonlinear) spacial operator respectively, $\mathcal{P}$ is the projection operator to the resolved scales and $\vec{u_0}$ and $\mathcal{N}_0$ are the numerical solution and the discretized Navier-Stokes operator respectively. Assuming $\vec{e} = 0$ initially, the term

$$\vec{Er} \equiv (\mathcal{P}\mathcal{N} - \mathcal{N}_0\mathcal{P})\vec{u}, \tag{9}$$

is defined as the 'error'. Periodic boundary conditions are assumed and this error is transformed to Fourier space replacing derivatives with wavevectors, and approximate derivatives with modified wavenumber vectors. Ghosal then identifies terms in the resulting $Er_i(\mathbf{k})$ due to truncation error and to aliasing error. Focusing on the truncation error, the assumption is made of statistical isotropy, and spherical averaging is employed in calculating the power spectrum, resulting in an expression which is a function of the magnitude wave vector $\kappa = |\mathbf{k}|$. During the averaging procedure, the familiar joint-normal hypothesis [2] is employed to eliminate third-and-higher order correlations. Via these steps, an expression for spectra of the truncation error energy is obtained,$\mathcal{E}^{(FD)}$, that takes the form

$$\begin{aligned}
\mathcal{E}^{(FD)}(k) = {} & [F_1(k) + F_2(k)] \left\{ \sum_{i,m,n} |\triangle_{imn}(\mathbf{k},\widetilde{\mathbf{k}})|^2 \right\}_\Omega \\
& + 2F_3(k) \left\{ \sum_{i,m,n,p} \frac{k_m k_p}{k^2} \triangle_{imn}(\mathbf{k},\widetilde{\mathbf{k}}) \triangle^*_{ipn}(\mathbf{k},\widetilde{\mathbf{k}}) \right\}_\Omega \\
& + F_4(k) \left\{ \sum_{i,m,n,p,q} \frac{k_m k_p k_n k_q}{k^4} \triangle_{imn}(\mathbf{k},\widetilde{\mathbf{k}}) \triangle^*_{ipq}(\mathbf{k},\widetilde{\mathbf{k}}) \right\}_\Omega \\
& + 2\nu^2 E(k) \left\{ \left| \tilde{k}^2 - k^2 \right|^2 \right\}_\Omega ,
\end{aligned} \tag{10}$$

where

$$I_m = k \int_0^\infty d\xi \int_{|\xi-1|}^{\xi+1} d\eta E(k\xi) E(k\eta) W_m(\xi,\eta), \tag{11}$$

$$\begin{aligned}
F_1(k) &= \tfrac{1}{16}[7I_4 + 6I_3 - 2I_2 + 5I_1], & W_1(\xi,\eta) &= \tfrac{1}{\xi\eta}, \\
F_2(k) &= \tfrac{1}{16}[-3I_4 + 2I_3 + 2I_2 - I_1], & W_2(\xi,\eta) &= \tfrac{\left(1-\xi^2-\eta^2\right)^2}{4\xi^3\eta^3}, \\
F_3(k) &= \tfrac{1}{16}[-15I_4 - 6I_3 + 2I_2 + 3I_1], & W_3(\xi,\eta) &= \tfrac{(1+\xi^2-\eta^2)^2}{4\xi^3\eta}, \\
F_4(k) &= \tfrac{1}{16}[45I_4 - 30I_3 - 6I_2 + 7I_1], & W_4(\xi,\eta) &= \tfrac{\left[1-\left(\xi^2-\eta^2\right)^2\right]^2}{16\xi^3\eta^3},
\end{aligned} \tag{12}$$

$$\triangle_{imn}\left(\mathbf{k},\tilde{\mathbf{k}}\right) \equiv P_{imn}(\tilde{\mathbf{k}}) - P_{imn}(\mathbf{k}), \tag{13}$$

$$P_{imn}(\mathbf{k}) = \left\{ \begin{array}{cc} (k_n\Pi_{im} + k_m\Pi_{in})/2 & \text{if } \mathbf{k} \neq \mathbf{0}, \\ 0 & \text{otherwise} \end{array} \right\}, \tag{14}$$

$$\Pi_{ij} = \delta_{ij} - k_i k_j / k^2, \tag{15}$$

and $\{\quad\}_\Omega$ denotes a spherical average in wavenumber space. This expression gives, as a function of the modified wavenumber and assumed energy spectra of the flow, a measure of the truncation error that is introduced on the resolved scales by the choice of the numerical representation of the derivatives. As such it provides an ideal way to evaluate the performance of different center-difference stencils in the numerical simulation of turbulent flow.

2.3 TCD Stencils for LES: 7-point, 5-point

For a given stencil width and order of accuracy, our approach is to define the TCD stencil as the one which minimizes the total truncation error on the resolved scales,

$$\text{Total Error}(\alpha) = \int_0^{\frac{\pi}{\Delta x}} \mathcal{E}^{(\text{FD})}(\kappa, \tilde{\kappa}(\kappa,\alpha)) d\kappa. \tag{16}$$

Assuming that the majority of the dissipation takes place on subgrid scales, we put $\nu = 0$ in (10). In order to optimize the center-difference stencils with respect to (16), it is necessary to choose a unique energy spectra of the form given in (7). The values $a = 2.682$ and $b = 0.417$ were used to place $\pi/\Delta x$ in the inertial range of (7). The resolved portion of the resulting spectra, $\kappa < \pi/\Delta x$, then includes the beginning of the energy-cascade part of κ-space. This is compatible with the goal of performing LES calculations. These values place the maxima at $\kappa = 1$. We remark that the results (*ie* α) of the optimization

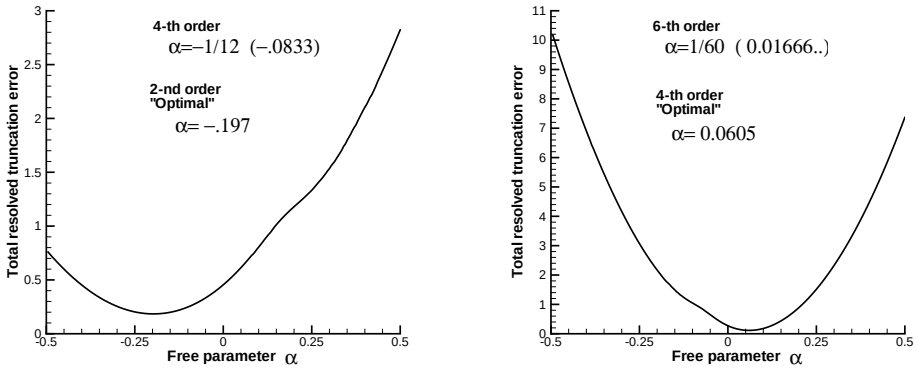

(a) 5-point (b) 7-point

Fig. 1. Total resolved truncation error as a function of the free parameter α

were found to be rather insensitive to the particular form (values of a and b) of (7). The total truncation error on the resolved scales (16), was evaluated numerically over a range of the free parameter α for both the 5-point and 7-point stencils. It was found to indeed have a minimum as shown in Figure 1.

	Optimized	Standard
d_1	0.894	2/3
d_2	-0.197	-1/12
d_3	0	0

Table 1
5-point stencils,2nd and 4th order

	Optimized	Standard
d_1	0.969166	3/4
d_2	-0.343333	-1/10
d_3	0.0605	1/60

Table 2
7pt stencils, 4th and 6th order

The minimization procedure leads to a value of $\alpha = -.197$ for a 5-point stencil and $\alpha = 0.0605$ for the tuned (ie optimal) 7-point stencil; see Tables 1 and 2 for a comparison of the standard and optimal stencils. An examination of the modified wavenumber shows improvement in the approximation of the derivative over a wider range of wavenumbers as shown in Figure 2.

2.4 LES of Decaying Compressible Turbulence

Using compact finite-difference Padé schemes and a structure-based model [19] for the subgrid stresses, Kosovic *et. al.* [8] obtained excellent agreement with direct numerical (DNS) computations of decaying isotropic compressible turbulence with a turbulent Mach number $M_t \sim 0.4$. Here we report the results of repeating the same LES calculations with the same subgrid model, initial conditions, and code. We change only the numerical derivative scheme to use

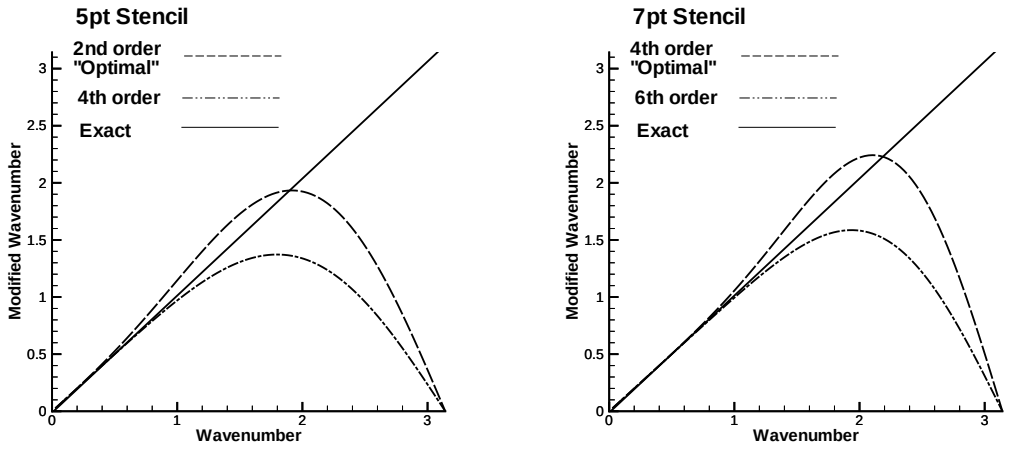

(a) 5-point (b) 7-point

Fig. 2. A comparison of modified wavenumbers $\tilde{\kappa}$ from optimized and non-optimized stencils

either standard center-difference or the TCD in place of the Padé method. In this way the direct affect of the TCD stencil is investigated.

As outlined in [8], a density weighted (Favre-filtered) form of the Navier-Stokes equation is utilized and a stretched vortex subgrid-scale model provides both the subgrid stresses τ_{ij} and the turbulent temperature flux q_i; triple correlations and the subgrid viscous work are assumed small and are neglected. References [8,14], as well as [19] provide details of the model; briefly, within each cell the stress is given by

$$\tau_{ij} = \overline{\rho} K(\delta_{ij} - e_i^v e_j^v), \qquad K = \int_{k_c}^{\infty} E(k)dk, \tag{17}$$

where $\overline{\rho}K$ is the subgrid energy, $\mathbf{e^v} = (e_1^v, e_2^v, e_3^v)$ is the unit vector of the subgrid vortex axis, and $E(k)$ is the energy spectra resulting from assuming a Lundgren type stretched vortex

$$E(k) = \mathcal{K}_o \epsilon^{2/3} k^{-5/3} \exp[-2k^2\nu/(3|a|)], \tag{18}$$

where $\mathcal{K}_o$ as the Kolmogorov prefactor, ϵ is the local cell-averaged dissipation, and a represents the axial strain along the subgrid vortex axis. Assuming that, on the subgrid scale, temperature maybe modeled as a passive scalar and using the resolved scale temperature $\tilde{T}$, the turbulent temperature flux is computed using a tensor-diffusivity model

$$q_i = \frac{1}{2} \triangle K^{1/2} (\delta_{ij} - e_i^v e_j^v) \frac{\partial \tilde{T}}{\partial x_j}, \tag{19}$$

where $\triangle$ is the local mesh size. The numerical method is detailed in Sam-

taney *et. al.* [15]: No explicit dealiasing of the nonlinear terms is performed, instead the advective term is discretized using the skew-symmetric form and a spherical spectral filter is applied after each time step. Owing to the fact that the shear viscosity coefficient depends on the temperature as $\mu = T^{0.76}$, the viscous term is computed by applying the first derivative twice.

We compare LES results with the detailed calculations of decaying compressible turbulence at moderate turbulent Mach number [15]. In particular comparison is made with the representative study, case $D9$, DNS of turbulence in a periodic domain performed with a 10th-order Padé scheme and 256^3 grid points. The flow is characterized by an initial spectrum peak at $k_o = 4$ and turbulent Mach number of $M_t = 0.488$ with a Taylor Reynolds number of $Re_\lambda = 175$. As in [8] the initial conditions for 32^3 LES were obtained by filtering the DNS data using spectral filter with a cutoff wavenumber of $k_c = 16$ after approximately one eddy-turnover period in order to avoid initial transient associated with startup.

The results of the decay of the kinetic energy on the resolved scales are shown in Figure 3. The decay rates are significantly improved by using the TCD stencils. LES with non-optimal stencils (other values of the parameter α) can greatly over or under estimate the decay. While the decay rate was rather insensitive to the representation of the derivative used in the viscous term on the resolved scales, we mention that the computed spectra is nearly identical to that shown in [15] Figure 3 (a) with the caveat that the energy pile-up in the highest resolved wavenumbers can be greatly reduced by using spectral derivatives in the viscous term.

Ghosal's analysis pertains to incompressible flow, but the results of our numerical experiments demonstrate that these optimized center-difference stencils work well with weakly compressible flows. This may be explained in part by the observation that, while shocklets form in such a flow, the majority of the dissipation occurs in the solenoidal part of the velocity field. For the purpose of comparison a 32^3 run is shown in Figure 3 obtained from an LES calculation using formally 5th-order WENO with Roe's approximate Riemann solver. In this simulation, WENO effectively supplies all of the dissipation by means of large numerical diffusion.

3 Hybrid TCD-WENO Scheme

WENO schemes [7,11] excel at capturing moving discontinuities such as shock waves and contact surfaces, while reverting to formally high order in smooth regions by utilizing, at each location, a potentially unique stencil constructed from a superposition of upwind biased candidates. Unfortunately, these schemes

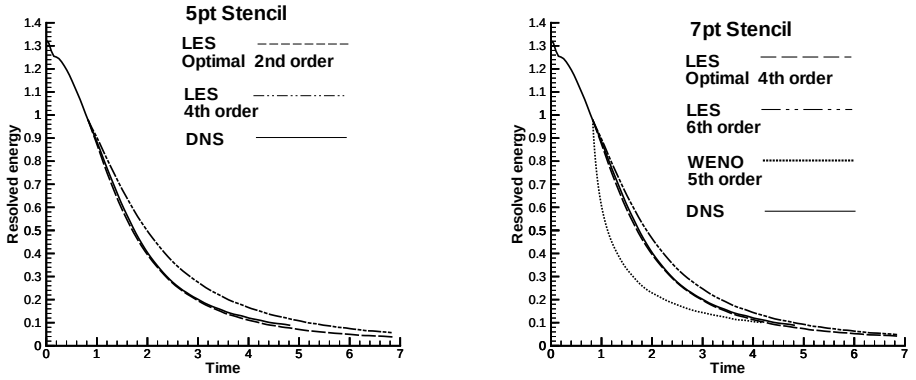

(a) 5-point (b) 7-point

Fig. 3. 32^3 LES calculations showing the decay of the kinetic energy on the resolved scales using the optimized stencils. The dark curve represents the DNS results of 256^3 Padé

introduce substantial numerical dissipation as well as phase errors. These problems can be related to two sources: WENO's 'optimal stencil', and the upwinding nature of the candidate stencils. Working within the WENO framework, several investigators have tried to address these shortcomings. Weirs and Candler [21] developed a symmetric WENO optimal stencil with low dissipation errors, which has been extended by Lin and Hu [10] additionally Wang and Chen [20] improved the dispersion relations for the candidate stencils. While these approaches all arguably lead to improved fidelity, they do not perform well in LES calculations for a subtle reason, namely, that even away from shocks and strong discontinuities, WENO does not consistently create a particular stencil, with the consequence that the dispersion relation is unpredictable. Worse yet, as WENO seldom obtains its optimal stencil, the upwinding bias of the candidate stencils often results in dissipation in the high wavenumbers which makes them poorly suited for LES, [12]. Hybrid schemes, [1,13], which utilize WENO type methods in regions of discontinuities and Padé derivatives elsewhere have been advanced to address this problem. Such methods have their own difficulties, such as formulating a criteria which determines when and where the Padé derivatives are to be used, and insuring that differences in dispersion relations where the different numerical methods meet do not generate excessive errors. Adams and Shariff [1] computed fluxes with an ENO scheme at discontinuities and standard Padé elsewhere, while Pirozzoli [13] used WENO and a modified upwinding Padé, presumably for stability or perhaps to damp such oscillations.

As a demonstration of the utility of our TCD stencils we construct a hybrid method using WENO at discontinuities and tuned center-difference in the smooth regions of the flow. To minimize the generation of noise at regions

where TCD transitions to WENO, the 'optimal stencil' is modified to match the TCD. We refer to such a WENO as tuned to blend well with the TCD.

3.1 Tuned WENO

We now outline how flux derivatives are computed with a tuned WENO method. In the hybrid scheme, such computations are to be performed at points where the flow is discontinuous or nearly so. Initially, the general flux $f(x)$ is split into two parts, one with a strictly non-negative derivative and the other non-positive: $f(x) = f^+(x) + f^-(x)$. In our calculations this splitting was done in characteristic space using a Roe-averaged Jacobian decomposition. Following the standard convention, our discussion will assume $f^+(x)$ and the superscript will be suppressed; formulas for $f^-(x)$ maybe obtained by symmetry about $x_{j+1/2}$.

In general, with WENO and other finite volume based methods, the procedure for computing the derivative at a the j-th location is to first interpolate flux values on the half grid points $\hat{f}_{j-1/2}$ and $\hat{f}_{j+1/2}$ and then form the difference

$$\frac{df}{dx} = \frac{1}{\triangle x}\left(\hat{f}_{j+1/2} - \hat{f}_{j-1/2}\right). \tag{20}$$

The interpolated values are the weighted sum of individual interpolations $q_k|_{j+1/2}$ each produced by a candidate stencil $a_{k,l}$ and combined according to coefficients w_k based on a fixed (referred to in the literature as 'optimal') set C_k but weighted by the local smoothness IS_k across each stencil. To compute WENO derivatives which will ideally revert to 7-point TCD in smooth regions requires the use of an additional candidate stencil when compared to the standard $r = 3$ (see [7]) method. Our approach follows that of Chandlier and Weirs [21], differing only in the values of C_k as we have a different target stencil. Specifically,

$$\hat{f}_{j+1/2} = \sum_{k=0}^{3} \omega_k q_k, \tag{21}$$

$$q_k|_{j+1/2} = \sum_{l=1}^{3} a_{k,l} f(x_{j-2+k+l}). \tag{22}$$

The weights are defined by

$$\alpha_k = \frac{C_k}{(\epsilon + IS_k)^2}, \tag{23}$$

and

$$\omega_k = \frac{\alpha_k}{\sum_{k=0}^{3} \alpha_k}, \tag{24}$$

where the smoothness measurement on the stencil k is IS_k given by

$$IS_k = \sum_{m=1}^{2} \int_{x_{j-1/2}}^{x_{j+1/2}} (\triangle x)^{2m-1} \left(\frac{\partial^m q_k}{\partial x^m} \right)^2 dx, \tag{25}$$

which may be computed as

$$IS_k = \sum_{m=1}^{2} \left(\sum_{l=1}^{2} d_{l,m,k} f(u_{j-1+l+k}) \right)^2, \tag{26}$$

and ϵ is a small regularization parameter. The values for the smoothness measurement coefficients $d_{l,m,k}$ and the candidate stencil coefficients $a_{k,l}$ are rather standard and are found in Tables 3-5. Where the flow is equally smooth across the candidate interpolation stencils, the superposition weights w_k tend to the values C_k. In standard WENO these values have been chosen so that that (20) will, in these areas, be of the highest possible formal order of accuracy; but for tuned WENO, values are chosen so that (20) will be equivalent to the TCD scheme. That is to say, $C_k s$ are chosen to satisfy

$$\sum_{k=1}^{k=3} d_k (f(x_{j+k}) - f(x_{j-k})) = \sum_{k=0}^{3} C_k \sum_{l=1}^{3} a_{k,l} (f(x_{j-2+k+l}) - f(x_{j-3+k+l})), \tag{27}$$

where the $d_k s$ are the center-difference values given in Table 2. Solving for C_k one obtains the values given in Table 3.

Optimal Weights				
k	0	1	2	3
C_k	0.18154396	0.31845603	0.31845603	0.18154396

Table 3
Interpolation superposition weights

$a_{k,l}$: Candidate Stencils			
k	$l=1$	$l=2$	$l=3$
0	2/6	-7/6	11/6
1	-1/6	5/6	2/6
2	2/6	5/6	-1/6
3	11/6	-7/6	2/6

Table 4
Candidate Stencil Coefficients

$d_{k,1,l}$: Smoothness Measures			
k	$l=1$	$l=2$	$l=3$
0	1/2	-4-2	3/2
1	-1/2	0	1/2
2	3/2	-4/2	1/2
3	-5/2	8/2	-3/2

$d^3_{k,2,l}$: Smoothness Measures			
all k	$\sqrt{13/12}$	$-2\sqrt{13/12}$	$\sqrt{13/12}$

Table 5
Candidate Stencil Smoothness coefficients

The previous section detailed the method of calculating flux derivatives with a tuned WENO scheme that in sufficiently smooth regions is equivalent to the TCD stencils that perform well in LES simulations. In principle WENO should go smoothly to TCD in flow regions away from shocks and other effective discontinuities, but in practice such a method alone is not sufficient as the resolved scale field of most turbulent flows are not sufficiently smooth to allow WENO to revert to this stencil. In fact repeating the 32^3 LES calculations of subsection 2.4 with tuned WENO produce results that are not perceptibly better than the standard WENO LES results shown in Figure 3 (b). Instead a switch is necessary to limit the regions of WENO activity to shocks and other discontinuities and to force explicit use of the TCD elsewhere. In his hybrid Padé-WENO scheme Pirozzoli [13] suggests a switch based on the criteria $|f(x_{j+1}) - f(x_j)| < \beta$ (for some value β) to determine when WENO is appropriate while Adams and Shariff [1] use a similar condition as well as test for a local maximum. We propose instead a scale independent measure of the variance $\lambda_{j+1/2}$ of the smoothness over the candidate stencils potentially used in the calculation of $\hat{f}_{j+1/2}$

$$\lambda_{j+1/2} = \frac{\max_k IS_k}{\min_k IS_k + \epsilon}, \tag{28}$$

where ϵ is a small regularization parameter, the value 10^{-4} was used. We require that tuned WENO is used in calculating the flux derivatives at points where $\lambda_{j+1/2}$ exceeds a given threshold λ_{max} as well as for the two neighboring points. The time stepping in all of our calculations was done with a fourth-order low storage Runge-Kutta method.

To demonstrate that such a switch is a viable approach Figure 4 shows the results using a threshold value of $\lambda_{max} = 20$ after one period ($t = 2$) of evolution of the one-dimensional wave equation

$$\frac{\partial u}{\partial t} + \frac{\partial u}{\partial x} = 0, \qquad 0 \leq x \leq 2, \tag{29}$$

with periodic boundary conditions. The analytic form of the exact wave in Figure 4 is that given by Jiang and Shu [7]. Note that with the increase in the number of grid points, not only does the solution become better resolved but the relative amount of WENO required decreases. This suggests that one could create similar hybrid methods with better computational performance then is presently achieved. The switching presented here is not intended to be an acceleration of WENO as the relatively expensive smoothness indicators are calculated at each point.

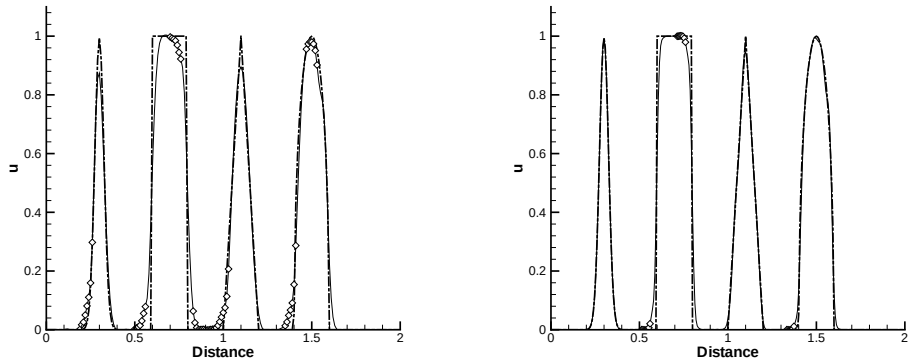

(a) N=200 pts. (b) N=300 pts.

Fig. 4. Linear one-dimensional wave equation with periodic boundary conditions and $\lambda_{max} = 20$. The thick dashed line represents the exact solution, the thin line shows the computed solutions on which locations where derivatives are computed by WENO are indicated by a $\diamond$.

4 Compressible Flow Examples Using the Hybrid Method

4.1 Equations of Motion

To demonstrate the hybrid TCD-WENO method, examples of one and two-dimensional flow containing shocks are presented. In particular the regions of the flow in which the different methods are used to compute the flux derivatives are indicated. This is done in part because of our interest in dispersion relations, and the belief that when performing LES, the less WENO the better from the standpoint of the overall fidelity of the flow.

Written in conservative form the two-dimensional Euler equations appear as

$$\frac{\partial \mathbf{q}}{\partial t} + \frac{\partial \mathbf{F}}{\partial x} + \frac{\partial \mathbf{G}}{\partial y} = 0, \tag{30}$$

in which $\mathbf{q} = (\rho, \rho u, \rho v, \rho e)^T$ and the flux vectors are given by

$$\mathbf{F} = \begin{pmatrix} \rho u \\ \rho u^2 + p \\ \rho uv \\ u(\rho e + p) \end{pmatrix}, \qquad \mathbf{G} = \begin{pmatrix} \rho v \\ \rho uv + p \\ \rho v^2 + p \\ v(\rho e + p) \end{pmatrix},$$

where ρ is the density, p the pressure, and u, v are the velocities in the x and y

directions respectively. The energy per unit mass, e is related to the velocities and pressure by

$$e = \frac{p}{\rho(\gamma - 1)} + \frac{1}{2}(u^2 + v^2). \tag{31}$$

As outlined in the previous section, the determination of when to use center-difference as apposed to tuned-WENO is based on the value of the measure $\lambda_{j+1/2}$. When applied to the two-dimensional Euler equations, $\lambda_{j+1/2}$ is calculated for each element of $\mathbf{F}$ and $\mathbf{G}$ and the determination to, for example, use WENO in the x-direction at a given location is based the maximum λ computed from the elements of $\mathbf{F}$ at that location.

We have found that in evolving the Euler equations, Gibbs-like ringing at sharp contact surfaces or shocks can be eliminated by requiring that WENO is used when $\lambda_{j+1/2}$ is greater than $\lambda_{max} = 150$ and, if it is necessary by this criteria to use tuned WENO at x_j, it is also used at x_{j-1} and x_{j+1} to insure that the transition from WENO to center-difference is smooth. Note that the value of λ_{max} differes from that in the one-dimensional wave example. In our experience this value is equation dependant, but appears to be constant across initial conditions and resolutions for a given equation. For example λ_{max} was fixed for all the one and two-dimensional calculations presented here.

4.2 One-Dimensional Shock and Entropy Wave Interaction

The evolution of the popular (eg [13,17,21]) test case representing a one-dimensional shock-entropy wave interaction is computed with the hybrid TCD-WENO scheme and the results are presented here. The initial conditions for the flow

$$(\rho, u, p) = \begin{cases} (3.857142, 2.629369, 10.333333) & x < 2, \\ (1 + 0.2\sin(5x), 0, 1) & x \geq 2, \end{cases} \tag{32}$$

result in the unsteady interaction of a Mach 3 shock with a sine entropy wave, and results at different times are presented in Figure 5. Note that the receding acoustic waves steepen behind the shock and give rise to shocklets, in particular the hybrid scheme recognizes this and uses tuned WENO when necessary. We find no perceptible ringing where tuned WENO switches to the TCD stencil.

4.3 Two-Dimensional Richtmyer-Meshkov Flow

The development of a two-dimensional Richtmyer-Meshkov instability is calculated as a further example of the hybrid TCD-WENO method. In this

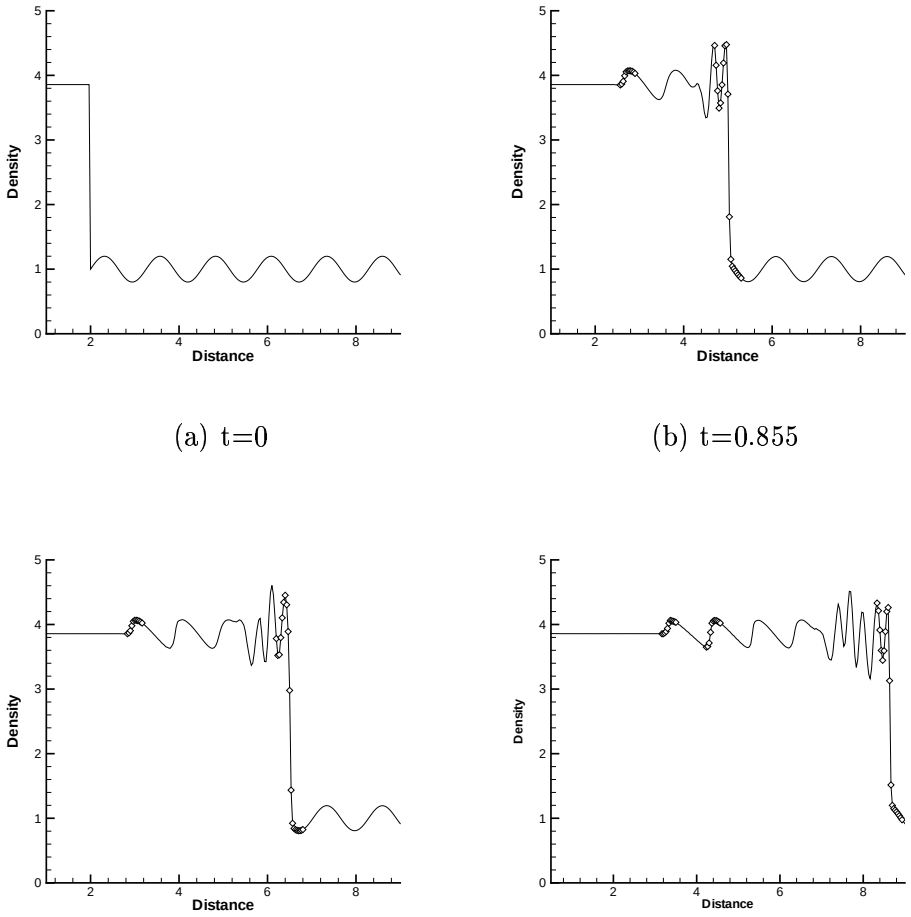

(a) t=0 (b) t=0.855

(c) t=1.277 (d) t=1.872

Fig. 5. Mach 3 shock and entropy wave interaction calculated with N=300 points and a $\gamma = 1.4$. Locations where derivatives are computed by WENO are indicated by $\diamond$.

simulation, a Mach 3 shock travels down (from left to right in our plots) a two-dimensional tube with non-dimensional length 23 and width 2.5, and encounters a density jump in the acquiescent gases of density ratio 1 : 2. At time $t = 0$, the shock was initially located at $x = 3.785$ and the interface contact surface was chosen to be at $x = 5.5$ and distorted from planar by a mulitmode perturbation with random phases. The density interface is not discontinuous but is smoothed across order 10 cells with a local tanh-like profile. The computational domain for calculations shown in Figure 6 was 1024x128 grid points. To eliminate the so-called carbuncle phenomenon in grid aligned shocks, the H-correction of Sanders *et al* [16] was employed when calculating the tuned WENO flux derivatives.

The interaction of the pressure gradient across the shock with the density gra-

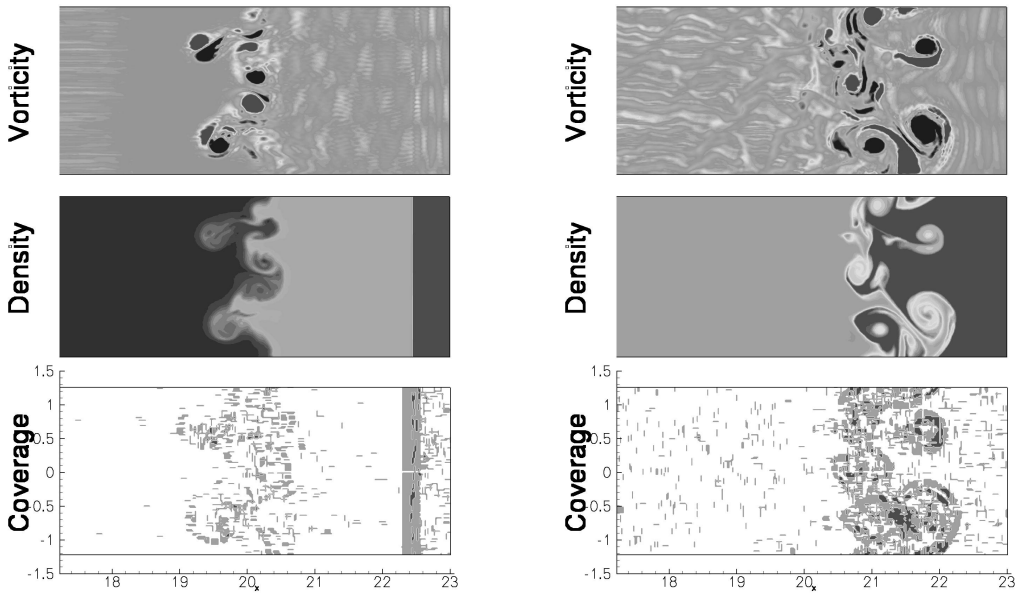

(a) t=9.56

(b) t=24.06

(c) t=38.54

(d) t=48.69.

Fig. 6. A Mach 3 Richtmyer-Meshkov instability evolution with an initial 1:2 density ratio and $\gamma = 1.4$ in both gases, computed on a domain of 1024x128, with 310x128 displayed. Vorticity, density and WENO coverage are shown at 4 successive times. For coverage, black regions correspond to WENO used in both directions, gray indicates WENO was used in either the x or y directions and white indicated that the TCD stencil operated in both directions.

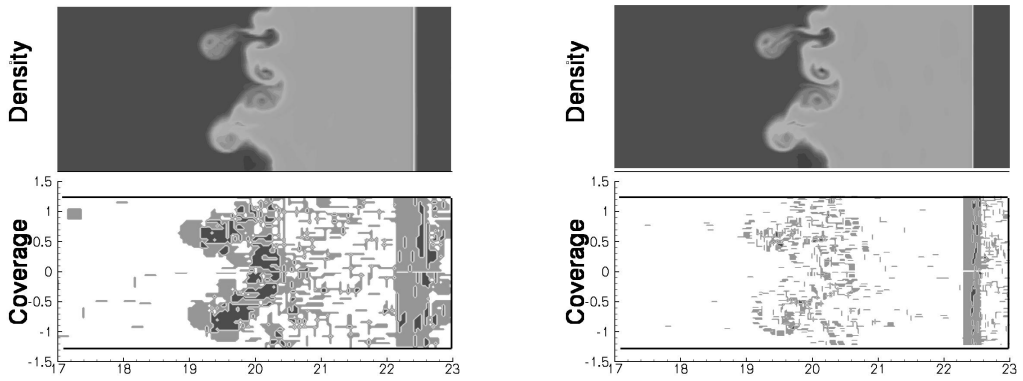

(a) 512x64 grid (b) 1024x128 grid

Fig. 7. A comparison of the coverage required at two different computational resolutions. For coverage key, see Figure 6

dient at the interface results in the deposition vorticity at this contact surface initiating mixing of the two gases. The transmitted shock continues down the tube, reflects off the far wall, and returns to re-shock the interface, leading to a further stage of mixing. The images shown in Figure 6 represent the development of this interface as well as the corresponding vorticity and a measure of the use of WENO. The gray regions in plots labeled *coverage* indicate locations where WENO was used in either the x or y flux derivative, while black regions correspond to WENO used in both directions. In nonshaded regions, the tuned TCD stencil operated in both directions. Figure 6 (a) shows the interface and the transmitted shock shortly after the initial interaction, but only the interface is visible in the later figures as the shock has reflected from the boundary at the right, re-shocked the interface and exited the displayed field of view. Note that the relative amount of WENO used in the area of the contact surface has increased between times (a) and (b), during which interval the contact surface has experienced re-shock resulting in sudden compression that steepens the local density gradients. As the flow continues to evolve, the dissipation inherent in WENO smooths the near discontinuities at the contact surface to the extent that less WENO is required in these regions, as can be seen in the later times (c) and (d).

As an example of the effect of grid size on the coverage, the computed solution vector at time (a) in Figure 6 was filtered from a resolution of 1024x128 to 512x64 and used as the initial condition for a lower resolution run of just a few time steps. Comparison of coverage between Figure 7 (a) and (b) indicates how the use of WENO in the hybrid scheme decreases in areas such as the contact surface as the resolution of the flow improves.

5 Conclusions

Motivated by bandwidth optimization combined with the idea of truncation error, we have presented tuned center-difference stencils which perform well in the resolved scale LES calculations of decaying compressible turbulence. In doing so, the role of the dispersion relation (ie modified wavenumber) was seen to play a more important role than the formal order of accuracy in the success of a scheme. We further integrated these simple stencils into a robust hybrid TCD-WENO scheme capable of simulating flows with strong shocks and contact surfaces. An investigation of the amount of WENO used in two-dimensional simulations of the evolution of a Richtmyer-Meshkov instability shows that increased resolution yields less WENO in the area of the contact surface. One could envision using techniques such as adaptive mesh refinement combined with our hybrid method to isolate the use of WENO to the capturable but unresolvable features such as strong shocks.

This work was supported by the Academic Strategic Alliances Program of the Accelerated Strategic Computing Initiative (ASCI/ASAP) under subcontract no. B341492 of DOE contract W-7405-ENG-48

References

[1] N.A. Adams and K. Shariff. A high-resolution hybrid compact-eno scheme for shock-turbulence interaction problems. *J. Comput. Phys.*, 127:27–51, 1996.

[2] G.K. Batchelor. Pressure fluctuations in isotropic turbulence. *Proc. Camb. Phil. Soc.*, 47:359, 1951.

[3] W.S. Don and D. Gottlieb. Spectral simulation of supersonic reactive flows. *SIAM J. Numer. Anal.*, 35,6:2370–2384, 1998.

[4] S. Ghosal. An analysis of numerical errors in large eddy simulations of turbulence. *J. Comput. Phys.*, 125,1:187–206, 1996.

[5] S. Ghosal. Mathematical and physical constraints on large-eddy simulations of turbulence. *AIAA J.*, 37,4:425–433, 1999.

[6] D. Gottlieb and J.S. Hesthaven. Spectral methods for hyperbolic problems. *J. Comput. Appl. Math.*, 128:83–131, 2001.

[7] G.-S. Jiang and C.-W. Shu. Efficient implementation of weighted eno schemes. *J. Comput. Phys.*, 126:202–228, 1996.

[8] B. Kosovic, D.I. Pullin, and R. Samtaney. Subgrid-scale modeling for large-eddy simulations of compressible turbulence. *Phys. Fluids A*, 14,4:1511–1522, 2002.

[9] S. Lele. Compact finite difference schemes with spectral like resolution. *J. Comput. Phys.*, 103,1:16–42, 1992.

[10] S.Y. Lin and J.J. Hu. Parametric study of weighted essentially non oscillatory schemes for computational aeroacoustics. *AIAA J.*, 39:371–379, 2000.

[11] X.-D. Liu, S. Osher, and T. Chan. Weighted essentially nonoscillatory schemes. *J. Comput. Phys.*, 115:200–212, 1994.

[12] R. Mittal and P. Moin. Suitability of upwind-biased finite difference schemes for large-eddy simulation of turbulent flows. *AIAA J.*, 35:1415–1417, 1997.

[13] S. Pirozzoli. Conservative hybrid compact-weno schemes for shock-turbulence interaction. *J. Comput. Phys.*, 178:81–117, 2002.

[14] D.I. Pullin. Vortex-based model for the subgrid flux of a passive scalar. *Phys. Fluids*, 12:2311, 2000.

[15] R. Samtaney, B. Kosovic, and D.I. Pullin. Direct numerical simulation of decaying compressible turbulence and shocklet statistics. *Phys. Fluids A*, 13,5:1415–1430, 2001.

[16] R. Sanders, E. Morano, and M.-C. Druguet. Multidimensional dissipation for upwind schemes: Stability and applications to gas dynamics. *J. Comput. Phys.*, 145:511–537, 1998.

[17] C.-W. Shu and S. Osher. Efficient implementation of essentially non-oscillatory shock-capturing schemes. ii. *J. Comput. Phys.*, 83:32, 1989.

[18] C.K. Tam and J.C. Webb. Dispersion-relation-preserving schemes for computational acoustics. *J. Comput. Phys.*, 107,2:262–281, 1993.

[19] T. Voelkl, D.I. Pullin, and D.C. Chan. A physical-space version of the stretched-vortex subgrid-stress model for large-eddy simulation. *Phys. Fluids A*, 12,7:1810–1825, 2000.

[20] Z.J. Wang and R.F. Chen. Optimized weighted essentially non-oscillatory schemes for linear waves with discontinuity. *J. Comput. Phys.*, 174:381–404, 2001.

[21] V.G Weirs and G.V. Candler. Optimization of weighted eno schemes for dns of compressible turbulence. *AIAA Paper*, 97-1940:1–11, 1997.

[22] M. Zhuang and R.F. Chen. Optimized upwind dispersion-relation-preserving finite difference scheme for computational aeroacoustics. *AIAA J.*, 36,11:2146–2148, 1997.

[23] D.W. Zingg. A review of high-order and optimized finite-difference methods for simulating linear wave phenomena. *AIAA J.*, 97-2008, 1997.